Proceedings of the 1999 IEEE/ASME
International Conference on Advanced Intelligent Mechatronics
September 19-23, 1999 • Atlanta, USA

Vision Based Active Sensor Using a Flexible Beam

Makoto KANEKO, Naoki KANAYAMA and Toshio TSUJI

Dept. of Industrial and Systems Engineering, Faculty of Engineering, Hiroshima University
1-4-1, Kagamiyama, Higashi-hiroshima, 739-8527, JAPAN
Phone:+81-824-24-7691, Fax:+81-824-22-7158
E-mail: kaneko@huis.hiroshima-u.ac.jp

Abstract— **This paper discusses vision based active sensing system, termed Vision Based Active Antenna(VBAA) composed of a camera, an insensitive flexible beam whose force-deformation characteristic is known, and an actuator for rotating the beam (see Fig. 2). The camera observes the beam deformation that includes the contact information, while the beam is in contact with an object. By solving a set of equations acquired through the camera, the sensor can detect the contact location and the contact force, even though the contact point is hidden by occlusion. For two particular versions, we show some experimental results to verify the basic idea.**

I. Introduction

The human sense of touch provides us with an important source of information about our surroundings. Because of its unique position at the interface between our bodies and the outside world, touch sensing supplies sensory data which helps us manipulate and recognize objects and warn of harmful situations. Many creatures including humans make good use of the tactile information they obtain through physical contact with external objects. Tactile sensing is very direct. It is not distorted by perspective, confused by external lighting or greatly affected by the material constitution or surface finish of objects. We humans use tactile information to maintain the posture of our bodies, to provide a warning of physical danger, and to monitor walking and grasping. Tactile sensing has the potential to fill a similar sensing role for robotics system.

So far, a number of tactile sensors have been proposed [1]–[11] and implemented to various robotic systems, especially grippers and multi-fingered robot hands. The use of tactile sensors for either recognizing the shape of object [7], [8], [9] or for detecting the local contact point between the sensor and an object [10], [11] has been discussed in the literature. Most of works implicitly assume that tactile sensor is placed already close to the target object and ready for starting a sensing action. In a general case, however, a robot has to begin by finding the target object itself before starting any tactile motion for recognizing the object's shape. Fig. 1(a) shows a sensing procedure for such a general case, where the mobile robot equips with tactile sensor but no other external sensor. S_1 and S_2 denote the starting points for finding the target object and for recognizing the object's shape, respectively. The sensing procedure is classified into two phases, namely, the approach phase where the robot approaches to the target object and the detection phase where the robot detects the shape of object by moving the tactile sensor. As seen from Fig. 1(a), this sensing procedure, especially the approach phase is particularly inefficient, since the robot has to repeat side-and-forward motions until it reaches the target object. On the other hand, suppose that the robot equips with a vision sensor as shown in Fig. 1(b). In such a case, the robot will be able to immediately recognize the rough position of object. Once the robot knows the rough information of object's position, it can quickly reach the starting position S_2. The same discussion will be applied even if we replace a mobile robot by a manipulator. Through the above two examples, we can learn that a global sensor such as vision is greatly helpful for guiding the robot to the target object. After such an approach phase, tactile sensor can take over its responsibility. Thus, a visual assistance during the approach phase is especially important when the robot obtains the surface profile of object through touch in an unstructured environment. Based on this consideration, we assume that a vision sensor is already implemented to assist tactile sensing.

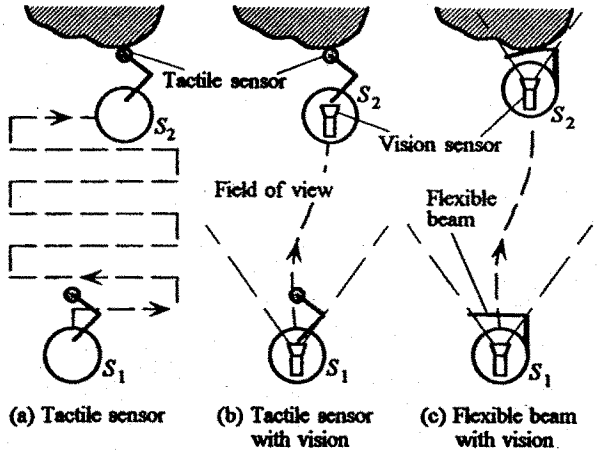

Fig. 1. Object sensing by the tactile sensor and the vision sensor.

In this paper, we discuss a vision based active sensor, where a vision system is used for the detection phase as well as the approach phase. For the detection phase, the vision observes the deformation of a flexible beam as shown in Fig. 1(c). When a flexible beam with a straight line is

0-7803-5038-3/99/$10.00 © 1999 IEEE

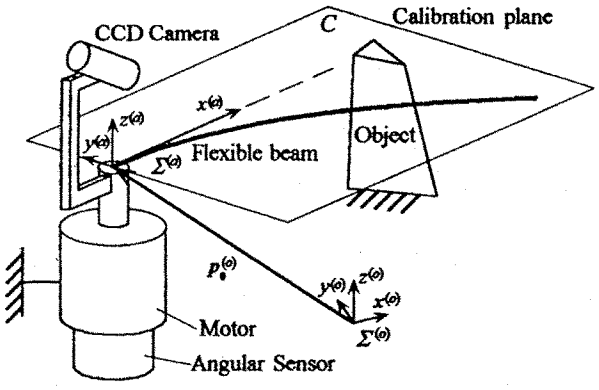

Fig. 2. An overview of the Vision Based Active Antenna.

in contact with an object, it deforms according to how much force is applied and where it makes contact. The beam keeps a straight line after the contact point, while it deforms a curved line between the base and the contact point. This means that the beam shape in contact with an object contains the contact information, such as contact point and contact force.

Under this background, we discuss an active sensing system called Vision Based Active Antenna (VBAA) composed of one insensitive flexible beam, one actuator to rotate the beam, one position sensor to measure the rotation angle of the beam and one CCD camera to observe the beam's shape, as shown in Fig.2. The actuator can be replaced either by driving wheels in a mobile robot or by joint actuators in a robot manipulator. Hereafter, we focus on the detection phase apart from the approach phase. An active motion is imparted to the beam while it is in contact with the object. The camera continuously observes the beam's shape. By observing the shape distortion from its original straight line position, the sensor system can detect any initial contact with the object. With a further active motion, the beam deforms according to the pushing angle, the contact location, and the object's stiffness. The pushing angle after contact can be regarded as input for the VBAA, and the beam's shape obtained through the CCD camera can be regarded as output. By the input-output relationship, we obtain a set of equations including the contact information. By solving them, the VBAA can detect the contact distance and the contact force. It is interesting to note that the VBAA can work even under occlusion where the contact point is hidden.

II. Main Assumptions

A. Main Assumptions

Main assumptions taken here are as follows:

Assumption 1: The deformation of beam is small enough to ensure that the beam's behavior obeys the force-deformation relationship based on linear theory.

Assumption 2: The object is stationary during active motions.

Assumption 3: The elongation of beam due to a unit axial force is negligibly small compared with the deflection due to a unit bending force.

Assumption 4: The beam is connected to the actuator shaft at the center of rotation.

Assumption 5: The beam has equal compliance in the place perpendicular to the longitudinal axis.

The VBAA needs the force-deformation relationship for evaluating the contact force. Assumption 3 implies that the beam is very stiff in its axial direction, while it is relatively compliant in non-axial direction. To simplify the discussions in this paper, we neglect the effect of an adapter with assumption 4. For practical application, however, the sensing system surely needs a proper adaptor for connecting an actuator with the beam, and such an adaptor has much stiffness compared with the beam.

B. Importance of the Beam Elasticity [12], [13]

Now, let us assume that the beam of the VBAA is rigid with scale. For the contact point detection, the CCD camera will be able to directly read the scale in contact with the object, if a good working condition is prepared for visual sensing. However, because of occlusion or lighting problems, providing good conditions for a vision system is not always easy and, the real contact point is often hidden or unreadable in ambiguous scene. When the beam makes contact with a compliant object, it is particularly difficult to find an exact contact point since it sinks into the surface. Furthermore, a rigid beam produces an impulsive force when it collides with an object with a speed. Thus, the VBAA using a rigid beam does not seem to work successfully for a practical environment. Let us now assume that the beam is an elastic one whose force-deformation behavior is known in advance. When such a beam makes contact with an object, it deforms according to the contact point, the pushing angle and the object's stiffness. The beam deforms between the base and the contact point, while the remaining part of the beam keeps in a straight line. By utilizing this information, the VBAA can evaluate the contact point. Later we will show that two arbitrary points on the beam are necessary and sufficient for determining the beam's unique shape if the deformation plane is given. In other words, if the sensor system can measure two points on the beam, the unique contact point is obtained. This is the great advantage in utilizing a flexible beam, since the sensor system can provide the contact point without requiring any information concerning the exact contact point.

III. Basic Equations

A. Relationship between Antenna and World Coordinates

Let $\boldsymbol{p}^{(a)}$ be the vector pointing a position on the antenna. The transformation from the antenna to the world coordinate system is given by

$$\boldsymbol{p}^{(o)} = \boldsymbol{p}_0^{(o)} + R_a^o \boldsymbol{p}^{(a)}, \quad (1)$$

$$\boldsymbol{p}^{(a)} = (x^{(a)}, y^{(a)}, z^{(a)})^T, \quad (2)$$

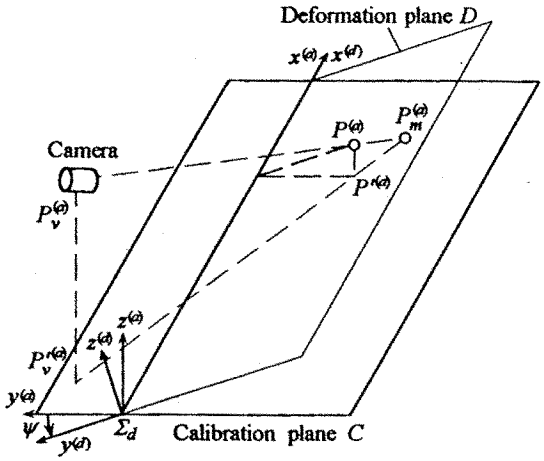

Fig. 3. A point projected to calibration plane C.

$$\boldsymbol{p}_0^{(o)} = (x_0^{(o)}, y_0^{(o)}, z_0^{(o)})^T, \quad (3)$$

$$\boldsymbol{R}_a^o = \begin{bmatrix} \cos\phi & -\sin\phi & 0 \\ \sin\phi & \cos\phi & 0 \\ 0 & 0 & 1 \end{bmatrix}, \quad (4)$$

where $\boldsymbol{p}_0^{(o)}$, ϕ and $\boldsymbol{R}_a^o$ denote the position vector between the origins of two coordinate systems, the angle for the motor and the rotational matrix from $\Sigma^{(a)}$ to $\Sigma^{(o)}$, respectively. Hereafter, we focus on the position sensing on the antenna coordinate system.

B. Relationship between Deformation Plane and Observing Point

We define the deformation plane $\mathcal{D}$ and the calibration plane C as shown in Fig. 3, where ψ denotes the inclination angle of the deformation plane with respect to the calibration plane. The deformation plane $\mathcal{D}$ corresponds to $x^{(d)}y^{(d)}$ plane in the deformation coordinate system $\Sigma^{(d)}$. For our simplicity, the calibration plane C is so chosen that it may be coincide with the $x^{(a)}y^{(a)}$ plane in the antenna coordinate system $\Sigma^{(a)}$. Note that we can obtain a position on C through the vision system.

A point $(x^{(d)}, y^{(d)}, 0)$ in the deformation coordinate system is transformed into the antenna coordinate system by the following relationship

$$\begin{pmatrix} x^{(a)} \\ y^{(a)} \\ z^{(a)} \end{pmatrix} = \begin{pmatrix} x^{(d)} \\ y^{(d)}\cos\psi \\ y^{(d)}\sin\psi \end{pmatrix}. \quad (5)$$

Suppose that a point $(x^{(a)}, y^{(a)}, z^{(a)})$ on the antenna is transformed by $(x_m^{(a)}, y_m^{(a)}, 0)$ on C. Under such a condition, $\triangle P_m^{(a)} P_v^{(a)} P_v'^{(a)}$ and $\triangle P_m^{(a)} P'^{(a)} P^{(a)}$ become similar each other as shown in the Fig. 3. This similarity relationship is given by

$$\begin{pmatrix} x_m^{(a)} - x^{(a)} \\ y_m^{(a)} - y^{(a)} \end{pmatrix} = \frac{z^{(a)}}{z_v^{(a)}} \begin{pmatrix} x_m^{(a)} - x_v^{(a)} \\ y_m^{(a)} - y_v^{(a)} \end{pmatrix}. \quad (6)$$

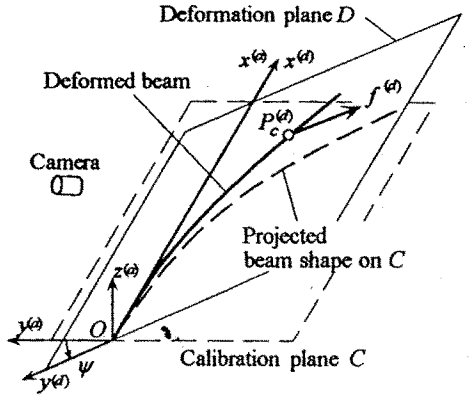

Fig. 4. Definition of the deformation plane.

Replacing eq.(5) into eq.(6), we obtain the following relationship

$$x^{(d)} = x_m^{(a)} - \frac{y_m^{(a)}(x_m^{(a)} - x_v^{(a)})\sin\psi}{z_v^{(a)}\cos\psi + (y_m^{(a)} - y_v^{(a)})\sin\psi}, \quad (7)$$

$$y^{(d)} = \frac{z_v^{(a)} y_m^{(a)}}{z_v^{(a)}\cos\psi + (y_m^{(a)} - y_v^{(a)})\sin\psi}. \quad (8)$$

C. Deformation of antenna on C

We first note that the antenna under a contact force deforms in a plane as shown in Fig. 4. The antenna shape is given by the following equations on $\mathcal{D}$

Curved part $(0 \le x^{(d)} \le x_c^{(d)} \le L)$

$$y^{(d)} = \frac{f^{(d)}}{6EI}(3x_c^{(d)} - x^{(d)})\{x^{(d)}\}^2, \quad (9)$$

Linear part $(0 < x_c^{(d)} \le x^{(d)} \le L)$

$$y^{(d)} = \frac{f^{(d)}}{6EI}(3x^{(d)} - x_c^{(d)})\{x_c^{(d)}\}^2, \quad (10)$$

where

$$f^{(d)} \equiv \sqrt{\{f_y^{(a)}\}^2 + \{f_z^{(a)}\}^2}, \quad (11)$$

$x_c^{(d)}$, L, E and I denote the contact point, the total length of the antenna, Young's modulus of elasticity and the second moment of area, respectively. Although eq.(11) does not include $f_x^{(a)}$ component, it should be small under a simple pushing motion to an object by a flexible beam. By considering this, we assume $f^{(d)} \approx \|\boldsymbol{f}^{(a)}\|$. In summary, eqs.(7), (8), (9) and (10) are a set of basic equations providing the contact information.

IV. Solutions of Basic Equations

A. ψ is known

There are two cases where ψ is known. When a knife-edged object is placed perpendicular to the calibration plane C, the deformation plane $\mathcal{D}$ coincides with C. This holds $\psi = 0$. The other case is expected for the beam

whose elasticity is not uniform but limited in a particular direction. A flat scale made by plastic is a good candidate for this kind of beam. For such a beam, the deformation plane $\mathcal{D}$ never changes irrespective of the direction of contact force. Therefore, ψ is determined uniquely.

When ψ is known, we can easily compute $(x^{(d)}, y^{(d)})$ from the measured point $(x_m^{(a)}, y_m^{(a)})$ by utilizing eqs.(7) and (8). Let us assume that we get two points $(x_1^{(d)}, y_1^{(d)})$ and $(x_2^{(d)}, y_2^{(d)})$ through a vision.

A.1 Two points from the curved part

From eq.(9), we can obtain the following two equations.

$$y_1^{(d)} = \frac{f^{(d)}}{6EI}(3x_c^{(d)} - x_1^{(d)})\{x_1^{(d)}\}^2, \quad (12)$$

$$y_2^{(d)} = \frac{f^{(d)}}{6EI}(3x_c^{(d)} - x_2^{(d)})\{x_2^{(d)}\}^2, \quad (13)$$

where $x_c^{(d)}$ should satisfy the condition of $0 < x_1^{(d)} < x_2^{(d)} \leq x_c^{(d)} \leq L$. From eq.(12) and (13), we can easily derive the unique set of solutions in $0 < x_1^{(d)} < x_2^{(d)} \leq x_c^{(d)}$ as follows,

$$f^{(d)} = 6EI\frac{\{x_2^{(d)}\}^2 y_1 - \{x_1^{(d)}\}^2 y_2^{(d)}}{\{x_1^{(d)}\}^2\{x_2^{(d)}\}^2(x_2^{(d)} - x_1^{(d)})}, \quad (14)$$

$$x_c^{(d)} = \frac{\{x_1^{(d)}\}^3 y_2^{(d)} - \{x_2^{(d)}\}^3 y_1^{(d)}}{3(\{x_1^{(d)}\}^2 y_2^{(d)} - \{x_2^{(d)}\}^2 y_1^{(d)})}. \quad (15)$$

Note that $x_2^{(d)} - x_1^{(d)} \neq 0$, $\{x_1^{(d)}\}^2 y_2^{(d)} - \{x_2^{(d)}\}^2 y_1^{(d)} \neq 0$, $x_1^{(d)} \neq 0$, $x_2^{(d)} \neq 0$ under $0 < x_1^{(d)} < x_2^{(d)} \leq x_c^{(d)}$.

A.2 Two points from the linear part

In this case, we can obtain the following two equations.

$$y_1^{(d)} = \frac{f^{(d)}}{6EI}(3x_1^{(d)} - x_c^{(d)})\{x_c^{(d)}\}^2, \quad (16)$$

$$y_2^{(d)} = \frac{f^{(d)}}{6EI}(3x_2^{(d)} - x_c^{(d)})\{x_c^{(d)}\}^2, \quad (17)$$

where $x_c^{(d)}$ should satisfy the condition of $0 < x_c^{(d)} \leq x_1^{(d)} < x_2^{(d)} \leq L$. From eq.(16) and (17), we can introduce the unique set of solutions in $0 < x_c^{(d)} \leq x_1^{(d)} < x_2^{(d)}$ as follows,

$$f^{(d)} = 2EI\frac{-(y_1^{(d)} - y_2^{(d)})^3}{9(x_2^{(d)} - x_1^{(d)})(x_1^{(d)} y_2^{(d)} - x_2^{(d)} y_1^{(d)})}, \quad (18)$$

$$x_c^{(d)} = \frac{3(x_1^{(d)} y_2^{(d)} - x_2^{(d)} y_1^{(d)})}{y_2^{(d)} - y_1^{(d)}}. \quad (19)$$

Note that $x_2^{(d)} - x_1^{(d)} \neq 0$, $y_2^{(d)} - y_1^{(d)} \neq 0$, $x_1^{(d)} y_2^{(d)} - x_2^{(d)} y_1^{(d)} \neq 0$ under $0 < x_c^{(d)} \leq x_1^{(d)} < x_2^{(d)}$.

A.3 One from each of the curved and linear parts

Without loss of generality, we can assume $0 < x_1^{(d)} \leq x_c^{(d)} \leq x_2^{(d)}$ and $x_1^{(d)} \neq x_2^{(d)}$. In this case, eq.(9) and (10) exist for each point. From these equations, we obtain,

$$g_{cl}(x_c^{(d)}) = y_1^{(d)}\{x_c^{(d)}\}^3 - 3x_2^{(d)} y_1^{(d)}\{x_c^{(d)}\}^2 + 3\{x_1^{(d)}\}^2 y_2^{(d)} x_c^{(d)} - \{x_1^{(d)}\}^3 y_2^{(d)} = 0 \quad (20)$$

Equation (20) is the cubic equation with respect to $x_c^{(d)}$. From eq.(20), we can easily show eqs.(21) and (22) under $0 < x_1^{(d)} \leq x_c^{(d)} \leq x_2^{(d)}$, $x_1^{(d)} \neq x_2^{(d)}$ and $0 < f^{(d)}$,

$$\lim_{x_c^{(d)} \to -\infty} g_{cl}(x_c^{(d)}) = -\infty, \quad (21)$$

$$\lim_{x_c^{(d)} \to +\infty} g_{cl}(x_c^{(d)}) = +\infty. \quad (22)$$

Now, let us examine the sign of $g_{cl}(x_1^{(d)})$ and $g_{cl}(x_2^{(d)})$. $g_{cl}(x_1^{(d)})$ and $g_{cl}(x_2^{(d)})$ can be rearranged in the following forms:

$$g_{cl}(x_1^{(d)}) = \frac{f^{(d)}}{6EI}(x_c^{(d)} - x_1^{(d)})\{x_1^{(d)}\}^3\{(3x_2^{(d)} - x_1^{(d)})(x_c^{(d)} - x_1^{(d)}) + x_c^{(d)}(x_2^{(d)} - x_1^{(d)}) + 2x_c^{(d)}(x_2^{(d)} - x_c^{(d)})\}, \quad (23)$$

$$g_{cl}(x_2^{(d)}) = -\frac{f^{(d)}}{6EI}\{x_1^{(d)}\}^2(x_2^{(d)} - x_c^{(d)})\{x_c^{(d)}(2x_2^{(d)} + x_c^{(d)})(x_2^{(d)} - x_1^{(d)}) + 2x_c^{(d)} x_2^{(d)}(x_2^{(d)} - x_c^{(d)}) + 2\{x_2^{(d)}\}^2(x_c^{(d)} - x_1^{(d)})\}. \quad (24)$$

Under the condition of $0 < x_1^{(d)} \leq x_c^{(d)} \leq x_2^{(d)}$, $x_1^{(d)} \neq x_2^{(d)}$ and $0 < f^{(d)}$, we can show $g_{cl}(x_1^{(d)}) \geq 0$ and $g_{cl}(x_2^{(d)}) \leq 0$. Conditions (21), (22), $g_{cl}(x_1^{(d)}) \geq 0$ and $g_{cl}(x_2^{(d)}) \leq 0$ ensure that we always have one solution between $x_1^{(d)}$ and $x_2^{(d)}$, while there are three solutions over the whole range.

Thus, the uniqueness of solution is guaranteed for IV-A.1 through IV-A.3. We call this version 2D-VBAA, where the beam deforms on a given plane.

B. ψ is unknown

Let $(x_i^{(d)}, y_i^{(d)})$ $(i = 1, 2, 3)$ be the measured points. For $(x_1^{(d)}, y_1^{(d)})$ and $(x_2^{(d)}, y_2^{(d)})$, we have the relationship given by eq.(15), and the same way for $(x_1^{(d)}, y_1^{(d)})$ and $(x_3^{(d)}, y_3^{(d)})$. Therefore, we can obtain

$$\frac{\{x_1^{(d)}\}^3 y_2^{(d)} - \{x_2^{(d)}\}^3 y_1^{(d)}}{\{x_1^{(d)}\}^2 y_2^{(d)} - \{x_2^{(d)}\}^2 y_1^{(d)}} = \frac{\{x_1^{(d)}\}^3 y_3^{(d)} - \{x_3^{(d)}\}^3 y_1^{(d)}}{\{x_1^{(d)}\}^2 y_3^{(d)} - \{x_3^{(d)}\}^2 y_1^{(d)}}. \quad (25)$$

We can regard that eq.(25) is the nonlinear equation with respect to ψ, while it does not include ψ explicitly. For obtaining ψ numerically, we define $g_{3D}(\psi)$ as follows

$$g_{3D}(\psi) = \frac{\{x_1^{(d)}\}^3 y_2^{(d)} - \{x_2^{(d)}\}^3 y_1^{(d)}}{\{x_1^{(d)}\}^2 y_2^{(d)} - \{x_2^{(d)}\}^2 y_1^{(d)}} - \frac{\{x_1^{(d)}\}^3 y_3^{(d)} - \{x_3^{(d)}\}^3 y_1^{(d)}}{\{x_1^{(d)}\}^2 y_3^{(d)} - \{x_3^{(d)}\}^2 y_1^{(d)}}. \quad (26)$$

For example, $g_{3D}(\psi)$ is given in Fig. 5, where $g_{3D}(\psi) = 0$ provides the solution of ψ. Once ψ is given, both $x_c^{(d)}$ and $f^{(d)}$ are automatically obtained. From Fig. 5, we can see the uniqueness of solution by means of numerical analysis, while we can not prove it in a mathematical way.

We call this version 3D-VBAA where ψ is not given in advance.

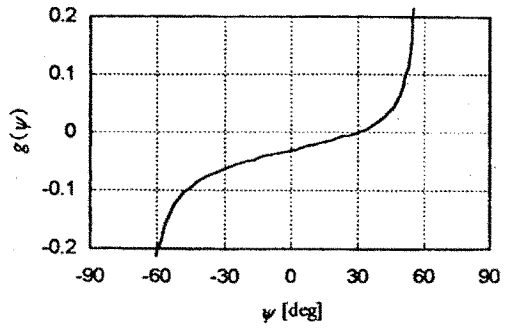

Fig. 5. A simulation result of the $g(\psi)$.

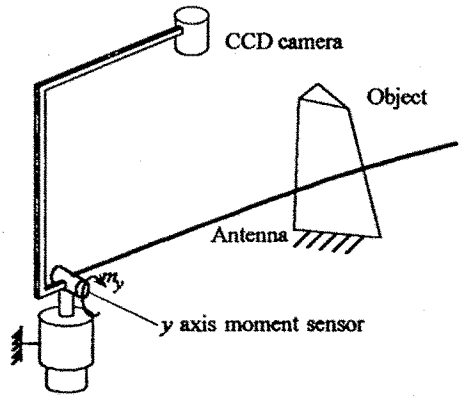

Fig. 6. The 3D-VBAA with a moment sensor.

C. An Extreme Case

While a general framework of 3D-VBAA is given in section IV-B, it is generally hard to solve the set of nonlinear equations and it is not guaranteed that we always have a unique solution for contact information. To cope with this, in this section, we discuss a specific version of 3D-VBAA, where both a vision and a moment sensor are in cooperated in the system as shown in Fig.6.

The vision sensor is placed so that the visual axis may be perpendicular to the calibration plane and the distance between the plane and the sensor may be long enough. Under such a sensor arrangement, we can regard that the deformation plane coincides with the calibration plane each other. Since we can remove ψ from the unknown parameters, the problem finally results in 2D one. From the discussion of 2D-VBAA, we can obtain both $(x^{(a)}, y^{(a)})$ component of contact position and $y^{(a)}$ component of contact force $f_y^{(a)}$. The $z^{(a)}$ directional force component can be evaluated by the moment sensor output. Since $m_y = x_c^{(a)} f_z^{(a)}$,

$$f_z^{(a)} = \frac{m_y}{x_c^{(a)}}. \tag{27}$$

By utilizing $f_y^{(a)}$ and $f_z^{(a)}$, we can estimate the beam displacement at the contact point as follows,

$$y_c^{(a)} = \frac{f_y^{(a)} \{x_c^{(a)}\}^3}{3EI}, \tag{28}$$

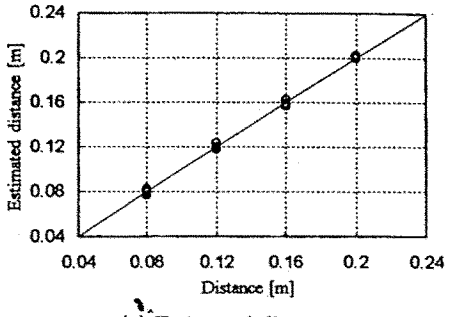

(a) Estimated distance

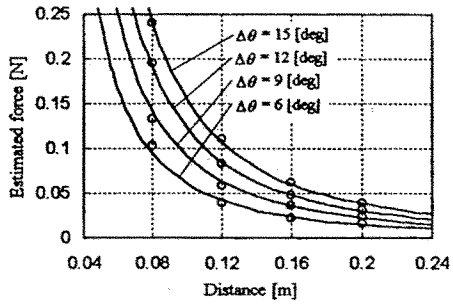

(b) Estimated contact force

Fig. 7. Experimental results for 2D-VBAA.

$$z_c^{(a)} = \frac{f_z^{(a)} \{x_c^{(a)}\}^3}{3EI}, \tag{29}$$

where $y_c^{(a)}$ and $z_c^{(a)}$ denote the beam displacements after it makes contact with the object. By estimating $y_c^{(a)}$ and $z_c^{(a)}$, we can obtain the current contact point which may differ from the initial one.

V. Experimental Verification

We used the experimental setup as shown in Fig. 6, where a knife-edge-like object is used. The image data are fed into the computer through a CCD camera with 512 × 512 dots and 8bits gray scale. For easily distinguishing the beam from the object, we use a white stainless beam with a diameter of 0.8mm and a length of 240mm. We believe that one of the big advantage of VBAA is that we can paint the beam so that it may be easily distinguished from the object. In order to suppress the frictional effect, we use an extremely slippery object.

A. 2D-VBAA

In this experiment, the output from the moment sensor is not utilized. Now, recall that the contact point for the 2D-VBAA can be obtained by observing two arbitrary points on the beam. However, if we compute the contact point by using two points only, it may include a large error by the digitizing error. In order to suppress such an error, we take an averaging process for the computed contact points by using more than 500 data. Figure 7 shows the experimental results, where (a) and (b) show the estimated contact distance and the contact force, respectively, and $\Delta\theta$ denotes

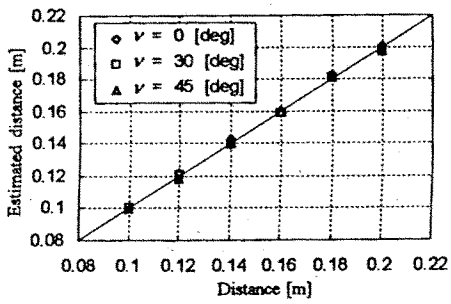

(a) Estimated distance

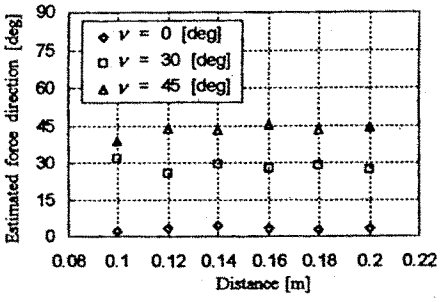

(b) Estimated force direction

Fig. 8. Experimental results for 3D-VBAA.

the pushing angle after making contact. The real lines and circles show the theoretical analysis and the experimental data, respectively. The agreement between analysis and experiments is fairly good.

The accuracy of the VBAA strongly depends on the thickness of the beam, the viewing area and the resolution of the captured picture. Through experiments, it is found that the best accuracy is obtained when the camera captured the tip part of the beam. This is probably because the tip part of the beam shifts more than the base part. Under the best case, we succeed in detecting the contact point with the accuracy of $\pm 2\%$.

B. 3D-VBAA with a moment sensor

Figure 8 shows experimental results where (a) and (b) show the estimated contact distance and the direction of the estimated contact force, respectively, and ν denotes the normal direction of the object surface. For this experiment, three objects with different normal direction are used. As shown in Fig.8(a), the estimation of contact distance can be executed with pretty high accuracy, even though the contact points do not exist on C. It can be seen from Fig.8(b) that the estimated direction of contact force almost coincides with that of normal direction of object's surface. This is because the frictional effect is reduced as much as possible in the experiment.

VI. Conclusion

In this paper, we discussed a sensing system Vision Based Active Antenna (VBAA) that can detect the contact force and the contact position between an insensitive flexible beam and an object, through the deformed flexible beam's shape. We introduce the basic equations for solving the contact point and the contact force. Even when the exact contact point is hidden by occlusion, the VBAA can still provide both the contact point and the contact force if two arbitrary points on the beam are observed for a 2D-VBAA or three points for a 3D-VBAA. While the vision system generally requires much computing power for analyzing the images, this system does not need. This is because it observes the shape of flexible beam only. We also showed some experimental results to verify this idea.

Another application for the VBAA is to use it as a force sensor. Even if the object is very tiny, for example microscopic object, this tactile system can be applied as a force sensor without utilizing any strain gauge. Thus, the VBAA may provide a kind of the force observation system.

ACKNOWLEDGMENT

This work was supported partly by the Grant-in-Aid for Scientific Research No.08650316 of the Ministry of Education in Japan.

References

[1] Buttazzo, G., P. Dario, and R. Bajcsy: Finger based explorations, *Intelligent Robots and Computer Vision: 5th in a Series*, David Casasent, ED., in *Proc. of SPIE*, Vol.726, pp.338–345, 1986.

[2] Begej, S.: Planar and finger-shaped optical tactile sensors for robotic applications, *IEEE J. Robotics and Automations*, Vol.4, No.5, pp.472–484, 1988.

[3] Cutkosky, M. R., and R. D. Howe: Dynamic tactile sensing, *Romansy'88: 7th CISM-IFToMM Symp. on the Theory and Practice of Robots and Manipulators*, Udine, Italy, 1988.

[4] Dornfeld, D., and C. Handy: Slip detection using acoustic emission signal analysis, *Proc. IEEE Int. Conf. on Robotics and Automations*, pp.1868–1875, 1987.

[5] Fearing, R. S., and T. O. Binford: Using a cylindrical tactile sensor for determining curvature, *Proc. IEEE Int. Conf. on Robotics and Automations*, pp.765–771, 1988.

[6] Howe, R. D., I. Kao, and M. R. Cutkosky: The sliding of robot fingers under combined torsion and shear loading, *Proc. IEEE Int. Conf. on Robotics and Automations*, pp.103–105, 1988.

[7] Dario, P., and G. Buttazzo: An anthropomorphic robot finger for investigating artificial tactile perception, *Int. J. Robotics Research*, Vol.6, No.3, pp.25–48, 1987.

[8] Brock, D. L., and S. Chiu: Environment perception of an articulated robot hand using contact sensors, *Proc. IEEE Int. Conf. on Robotics and Automations*, pp.89–96, 1987.

[9] Maekawa, H., K. Tanie, K. Komoriya, M. Kaneko, C. Horiguchi, and T. Sugawara: Development of a finger-shaped tactile sensor and its evaluation by active touch, *Proc. IEEE Int. Conf. on Robotics and Automations*, p.1327, 1992.

[10] Russell, R. A.: Closing the sensor-computer-robot control loop, *Robotics Age*, April, pp.15–20, 1984.

[11] Wang, S. S. M., and P. M. Will: Sensors for computer controlled mechanical assembly, *The Industrial Robot*, March, pp.9–18, 1978.

[12] Kaneko, M., N. Kanayama, and T. Tsuji: Vision Based Active Antenna, *Proc. of the 1996 IEEE Int. Conf. on Robotics and Automation*, pp.2555–2560, 1996.

[13] Kanayama, N., M. Kaneko, and T. Tsuji: On 3D Vision Based Active Antenna, *Proc. of the 1997 IEEE Int. Conf. on Robotics and Automation*, pp.143–148, 1997.